



ORIGINAL ARTICLE

Effect of the feeding mode of cross-linker and microcapsule on the corrosion resistance and hydrophobicity of composite coatings

Yan Bao ^{a,*}, Yan Yan ^{a,b}, Jing Zhang ^{a,b}, Jianzhong Ma ^{a,*}, Wenbo Zhang ^c,
Chao Liu ^c

^a College of Bioresources Chemical and Materials Engineering, Shaanxi University of Science and Technology, Xi'an 710021, China

^b National Demonstration Center for Experimental Light Chemistry Engineering Education, Shaanxi University of Science and Technology, Xi'an 710021, China

^c Shaanxi Collaborative Innovation Center of Industrial Auxiliary Chemistry and Technology, Shaanxi University of Science and Technology, Xi'an 710021, China

Received 12 July 2020; accepted 19 October 2020

Available online 29 October 2020

KEYWORDS

Metal coating;
Corrosion;
Polyacrylate;
Capsule;
Cross-linker

Abstract The interface combination of anti-corrosive materials and polymer matrix has a significant effect on the overall performance of the composite coating. However, past research has focused on blending anti-corrosive materials to improve the performance of the polymer matrix. Herein, we proposed a layer-by-layer spray-coating process to further enhance the reinforcing effect of anti-corrosive materials on the polymer matrix by changing their feeding modes. In this paper, taking waterborne polyacrylate (WPA) as an example, two kinds of reinforcement materials commonly used to improve the corrosion resistance of polymer matrix were introduced into the coating system and then applied to the tinplate: cross-linker and microcapsule. Firstly, five types of WPA composite coating systems were designed according to the feeding mode of aziridine cross-linker and the position of benzotriazole@zinc oxide microcapsules (BTA@ZnO MCs). Electrochemical impedance spectroscopy (EIS) and electrical equivalent circuits were used to evaluate the corrosion resistance of these composite coating systems and analyze their electrochemical processes. By spraying the mixture of WPA and aziridine crosslinker as the bottom layer and BTA@ZnO MCs as the top layer, the resulting composite coating exhibited higher corrosion resistance and hydrophobic prop-

* Corresponding authors.

E-mail addresses: baoyan@sust.edu.cn (Y. Bao), majz@sust.edu.cn (J. Ma).

Peer review under responsibility of King Saud University.



Production and hosting by Elsevier

<https://doi.org/10.1016/j.arabjc.2020.10.029>

1878-5352 © 2020 The Author(s). Published by Elsevier B.V. on behalf of King Saud University.

This is an open access article under the CC BY-NC-ND license (<http://creativecommons.org/licenses/by-nc-nd/4.0/>).

erties. Scanning electron microscope (SEM) and contact angle tests indicated that the feeding mode of aziridine cross-linker and the position of BTA@ZnO MCs played important roles in the compactness and hydrophobicity of the composite coating. Subsequently, the effects of the amount of aziridine cross-linker and BTA@ZnO MCs on the corrosion resistance and physical properties of the composite coating were further analyzed by EIS, water absorption test, contact angle test and atomic force microscopy (AFM). The significant improvement in the corrosion resistance of this composite coating was mainly attributed to the synergistic effect of highly cross-linked network structure and superhydrophobic surface.

© 2020 The Author(s). Published by Elsevier B.V. on behalf of King Saud University. This is an open access article under the CC BY-NC-ND license (<http://creativecommons.org/licenses/by-nc-nd/4.0/>).

1. Introduction

Metal corrosion is one of the most frequent destructive hazards and has aroused great concern in the academic community. To date, a method widely used for metal protection is to apply an organic coating on its surface. Current research has focused on the development of epoxy resins (Xia et al., 2019) and polyurethane resins (Mihelčič et al., 2019; Ye et al., 2019; Nardeli et al., 2020) because of their high adhesion and water resistance. However, most of them are solvent-based systems that are difficult to fully hydrate and posing a significant threat to the environment and human health. Therefore, there is an urgent need to develop and use waterborne resins to protect metals.

Acrylic resins have attracted widespread attention in the field of corrosion protection due to their ease of being water-based, excellent weathering and adhesion properties, outstanding chemical and abrasion resistance (Fu et al., 2014; Gao et al., 2020). However, the poor density and water resistance of waterborne acrylic resins limit their corrosion resistance (Song et al., 2017; Yao et al., 2017). In order to compensate these deficiencies, the chief way is to introduce cross-linkers or micro-nano particles into the polyacrylate matrix to fabricate a composite coating. For example, previous studies demonstrated that the multi-aziridine ring in the cross-linker reacted with the carboxylate (Xia and Larock, 2011) and hydroxyl (Li and Tang, 2016) groups in the polymer to form a higher cross-linked network while the curing process of aziridine increased the cross-linking densities and improved mechanical properties of the polymer matrix. In addition, it was proved that embedding micro-nano particles in the coatings was an effective method to improve corrosion resistance due to its filling and reinforcing effects (Zhu et al., 2019; Malucelli et al., 2013). Zhang et al. (2002) pointed out that modified nanoparticles with extremely strong activity could promote the cross-linking reaction of the resin and enhance the compactness of the coating, thereby improving the corrosion resistance of the waterborne resin. Similarly, it was reported that the modified ZnO nanoparticles were dispersed uniformly throughout the waterborne polyurethane coating to prevent the migration of corrosive species onto the substrate (Christopher et al., 2015). Especially in recent years, micro-nano capsules with stimulating responses have captured researchers' attention. The release of reactive polymers or corrosion inhibitors encapsulated in micro-nano capsules immediately repaired corrosion defects and achieved active corrosion protection of the coating (Chen and Fu, 2012; Chen et al., 2015).

Nevertheless, in most reports, micro-nano particles or micro-nano capsules are blended with a polymer matrix to form a coating on the metal substrate. The amount of anti-corrosive material introduced into the coating is quite limited. Also, since these materials are wrapped by polymer chains, their advantages in corrosion protection cannot be fully exploited. The layer-by-layer assembled technology with simplicity and versatility is expected to overcome the shortcomings of the above method by recombining various materials (i.e. cross-linkers, micro-nano materials, polymer matrices). Unfortunately, most of researches were focused only on the application of layer-by-layer assembled technology, but not on the optimization of construction technology. In other words, no research has been reported to improve the corrosion resistance of coatings by changing the position of micro-nano capsules and the feeding mode of cross-linker.

Therefore, based on our previous work, in which BTA@ZnO MCs were blended with WPA to form the composite coating (Bao et al., 2019), the combination of BTA@ZnO MCs and WPA and the optimization of construction technology by layer-by-layer assembled technology to obtain a coating with good corrosion resistance is the goal of this work. In addition, an aziridine cross-linker was introduced into the coating to enhance the bonding between BTA@ZnO MCs and WPA. Compared with our previous work, the dosage of BTA@ZnO microcapsules was increased greatly in this work. On the other hand, the introduction of aziridine cross-linker improved the compactness of composite coating. Thus, the corrosion protection of the composite coating was enhanced. Meanwhile, according to the feeding mode of the aziridine cross-linker and the position of BTA@ZnO MCs, five types of composite coating systems were designed and then applied to the tinplate. Among them, the composite coating system with the mixture of WPA and aziridine cross-linker as the bottom layer while BTA@ZnO MCs as the top layer has better corrosion protective properties. In order to evaluate the effects of the amounts of aziridine cross-linker and BTA@ZnO MCs on the physico-chemical properties of the composite coating and to explore the corrosion mechanism of the composite coating, electrochemical impedance spectroscopy (EIS) and physical properties of this coating system were further studied.

2. Experimental

2.1. Materials

The synthesis of BTA@ZnO MCs and WPA referred to our previous works (Bao et al., 2019; Bao and Chen, 2018).

Aziridine (C_3H_7N) was obtained from Hangzhou Palm Tech Development Co., Ltd., China. Ethanol (EtOH) was obtained from Tianjin Fuyu Fine Chemical Co., Ltd., China. Sodium chloride (NaCl) was provided by Tianjin Tianli Chemical Reagent Co., Ltd., China. Tinplates used for corrosion testing were purchased from Dongguan Weida Instrument Factory, China. All chemicals were used as received without further purified. Deionized water was used throughout the experiment.

2.2. Preparation of composite coating systems based on waterborne polyacrylate

The tinplates used were polished with 400 mesh and 800 mesh sandpapers in sequence to expose the iron substrate, and then placed in ethanol for ultrasonic cleaning for 30 min. Five types of composite coating systems were fabricated according to the difference in the feeding mode of aziridine cross-linker and the position of BTA@ZnO MCs, as shown in Table 1. Sample I is a composite coating obtained by spraying a mixture of WPA and BTA@ZnO MCs. Sample II is a composite coating obtained by spraying a mixture of WPA, BTA@ZnO MCs and aziridine cross-linker. Sample III is a composite coating obtained by spraying a mixture of WPA and aziridine cross-linker as the bottom layer and BTA@ZnO MCs as the top layer. Sample IV is a composite coating obtained by sequentially spraying WPA, aziridine cross-linker and BTA@ZnO MCs. Sample V is a composite coating obtained by spraying WPA as the bottom layer and a mixture of aziridine cross-linker and BTA@ZnO MCs as the top layer. A pure WPA coating was prepared as a blank sample. The spray gun was operated at a moving speed of 3–5 cm/s under compressed air (4–6 kPa working pressure) at room temperature. During spraying, the typical working distance was kept at 20 cm and the angle between the spray gun and the tinplate was 60°. After spraying, the sample was dried at 85 °C for 5 min and then dried at room temperature. The thickness of all composite coating systems were ~20 µm. The doses of aziridine cross-linker and BTA@ZnO MCs were varied in the coating system III and were determined to be 1, 3, 5, 7 mg/cm² and 0.8, 2.5, 4.2 mg/cm², respectively.

Table 1 Design of coating systems.

Coating system	Coating model	Spraying in Order
I		The mixture of WPA and BTA@ZnO MCs
II		The mixture of WPA, cross-linker and BTA@ZnO MCs
III		The mixture of WPA and cross-linker as the bottom layer, and BTA@ZnO MCs as the top layer
IV		WPA, cross-linker and BTA@ZnO MCs as single layer in sequence
V		WPA as the bottom layer, and the mixture of cross-linker and BTA@ZnO MCs as the top layer

2.3. Characterization

The surface morphologies of the studied coatings were observed with an S4800 scanning electron microscope (SEM) at an acceleration voltage of 20 kV. The surface topography of the coating was also examined by SPI-3800N-SPA400 atomic force microscopy (AFM).

The water absorption of the studied coatings was determined by the weight method. First, the composite coating was cut to a 1.5 × 1.5 mm sample and its weight was marked as m_0 . Then, the sample was immersed in deionized water for 24 h and the water on the surface of the sample was blotted with filter paper. The sample was weighted and labeled as m_1 . The water uptake rate was calculated as follows: water uptake rate (%) = $100 \times (m_1 - m_0)/m_0$. Three parallel samples were tested for each composite coating.

Contact angle of the studied coatings was measured with 5 µL deionized water droplet by the sessile drop method using an OCA20 contact angle meter at 25 °C. For each composite coating, the contact angle was taken the average value of at least three measurements in different regions. Fourier-transform infrared spectra (FT-IR) of the BTA@ZnO MCs, pure WPA coating and five composite coating systems were obtained using a Bruker VECTOR-22 FT-IR instrument (UK) in the range from 500 to 4000 cm⁻¹. The BTA@ZnO MCs were directly mixed with potassium bromide powder (spectrally pure), and compressed into a tablet for characterization. These coatings were scraped off the substrate and ground into powders. And then the powders were mixed with potassium bromide powder (spectrally pure), and compressed into tablets for characterization.

The corrosive resistance of the studied coatings was investigated by electrochemical methods and salt spray tests. The electrochemical properties of the samples immersed in 3.5% NaCl solution were detected by AMETEK electrochemical workstation. A three-electrode cell was used employing the coated tinplate as a working electrode with an exposed area of 5 cm², a saturated calomel electrode (SCE) and a platinum sheet as reference and counter electrodes, respectively. The spectra were measured over a frequency range of 10⁵–10⁻² Hz with an ac wave of 10 mV. Additionally, the corrosion protection performances of the samples were investigated by salt spray test. “X” line was scribed on the coating with a blade. Then, the samples were placed in a salt spray machine (HJ-YW60, Dongguan Hengjun Instrument Equipment Co., Ltd., China) and examined at 0, 2 and 5 h, respectively. The temperature in the salt spray machine was 35 °C. The salt spray solution was a 5% NaCl solution with a pH of 6.5–7.2. The salt spray deposition amount was 1–2 mL/80 cm².

3. Results and discussion

3.1. Anti-corrosive performance

EIS measurements were utilized to study the corrosion protection of the pure WPA coating and five types of composite coating systems on the metal substrate (Grundmeier et al., 2000; Zheludkevich et al., 2007). Generally, larger semicircle diameter and higher impedance modulus at low frequency symbolize a superior corrosion resistance feature (Ye et al., 2018). From the semicircle diameter and impedance modulus at low fre-

frequency of different coatings immersed in 3.5 wt% NaCl aqueous solution (Fig. 1A and B), the five types of composite coating systems exhibited better corrosion resistance than the pure WPA coating. Moreover, the corrosion performance of these composite coating systems showed an upward tendency as follows sequence: I < IV < V < II < III. It could be seen from Fig. 1C that all coating systems exhibited three time constants, implying that the corrosive medium penetrated through the micro pores in the coating and the corrosion reaction occurred on the metal surface. The peaks of phase angle at the logarithm of the frequency from 0 to 1 meant the formation of oxide layers and inhibitor protective films.

To explore the electrochemical process and quantitatively evaluate the corrosion resistance of different coatings, the EIS results were fitted to electrical equivalent circuits by Zsimpwin software. Two electrical equivalent circuits (circuit A for pure WPA coating and coating systems I, II, circuit B for coating system III, IV and V) in Fig. 2 were proposed after comparing the fitting parameters of various circuit models. Where, R_s refers to the resistance of the electrolyte between the counter electrode and the working electrode. R_c is the pore resistance of the coating due to electrolyte penetration or as areas where more rapid solution uptake occurs, i.e., preexisting holes or porous areas (Park and Park, 2014). It is a direct indicator of the corrosion protective performance of coating (Tian

et al., 2015). R_{ox} is the resistance of both oxide layers (Fe_2O_3 and Fe_3O_4) and protective films due to the inhibition effect of BTA (Shi et al., 2010). R_{ct} is the resistance to electron transfer across the metal surface, which varies inversely to the corrosion rate (Lu et al., 2017; Zhang et al., 2016). C_c represents the coating capacitance and is considered as a parameter to estimate the resistance to water penetration (Liu et al., 2018a,b). C_{dl} refers to the double-layer capacitance, reflecting the charge accumulation at the interface between the coating and the metal surface. Q , as a constant phase-angle element (CPE), denotes the deviation from pure capacitance. Q_{ox} refers to the charge accumulation on both oxide layers (Fe_2O_3 and Fe_3O_4) and inhibitor protective films. The Q in circuit B is used to instead of the capacitance (C) in circuit A because of different physical phenomena like surface roughness, inhibitor adsorption, porous layer formation, etc. (Cui et al., 2017). The pertinence between Q and C is described by n value, which is considered as pure capacitance as for n equal to 1 (Liang et al., 2018; Liu et al., 2018a,b).

Due to the hydrophilic nature and poor density of waterborne polyacrylate coating, the penetration process of corrosive medium in coatings was completed to reach saturation state in a short time (Liu et al., 2018a,b). On the one hand, when the corrosive medium was in contact with the metal surface, the corrosion reaction occurred on the metal surface. The

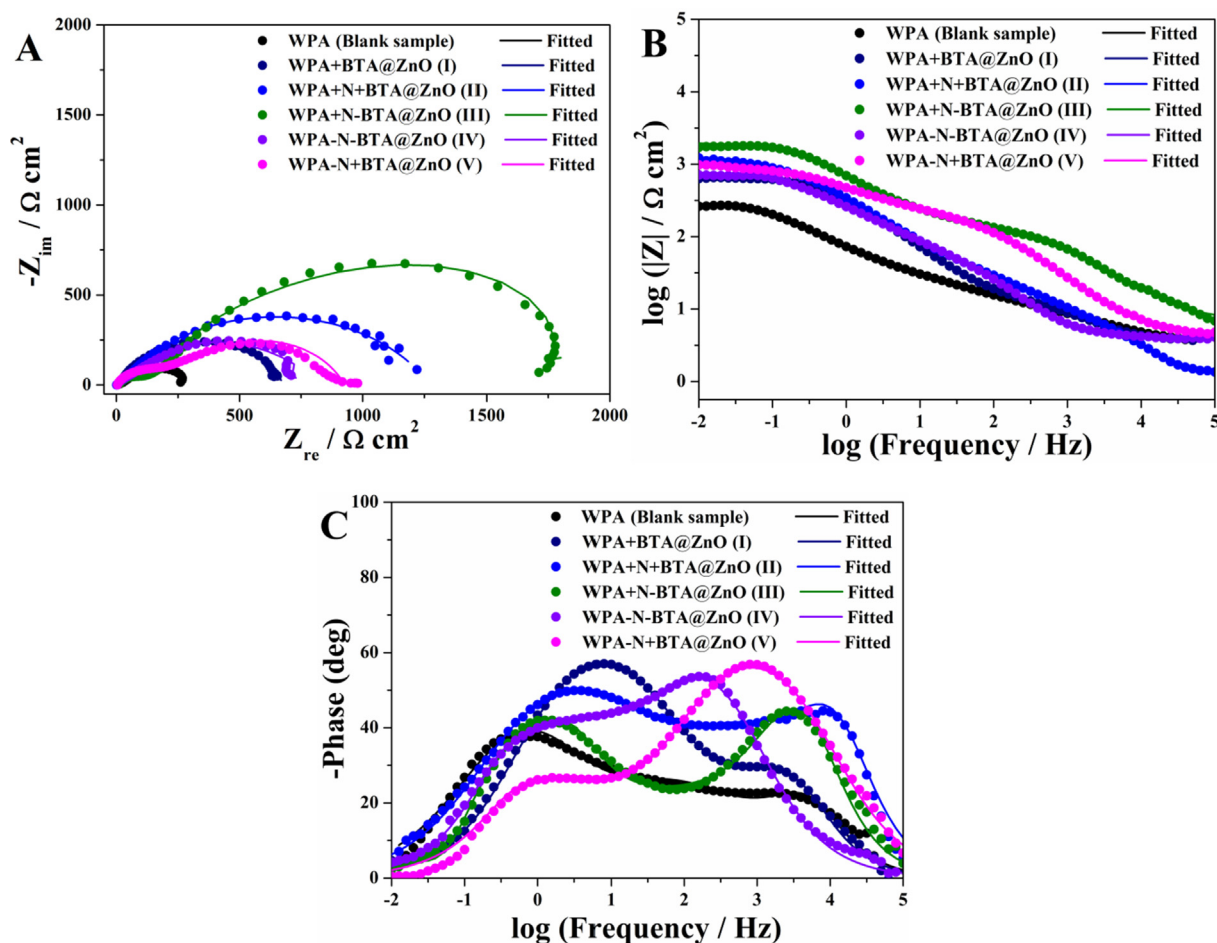


Fig. 1 Electrochemical impedance spectroscopy of the pure WPA coating and different composite coating systems immersed in 3.5 wt% NaCl aqueous solution at room temperature. Nyquist plots (A), Bode plots (B and C).

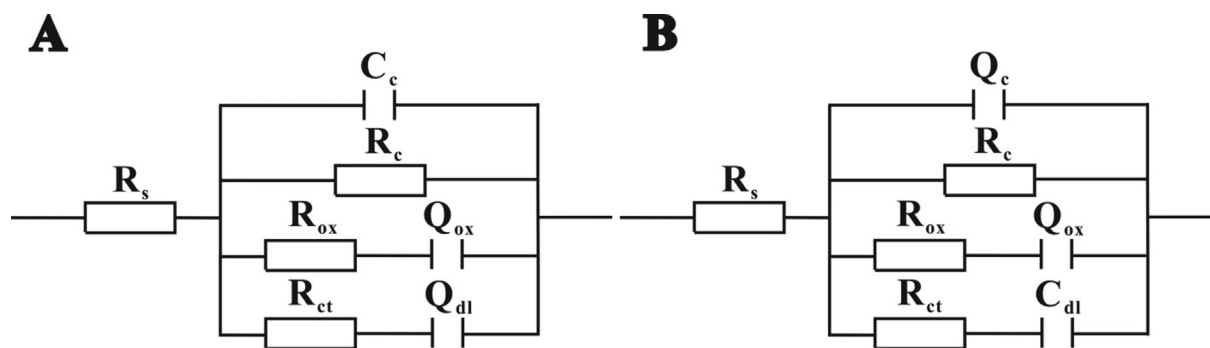


Fig. 2 Electrical equivalent circuit diagrams of the pure WPA coating, composite coating systems I and II (circuit A: $R(CR(QR)(QR))$), composite coating systems III, IV and V (circuit B: $R(QR(QR)(CR))$).

Fe ions were then converted into Fe_2O_3 and Fe_3O_4 to form oxide layers on the metal surface, thereby protecting metal. On the other hand, the BTA was released from the microcapsules because the corrosive medium penetrated. The released BTA with nitrogen heteroatoms shared their electrons with unoccupied orbitals of surface metal atoms (Javadi et al., 2019) and formed a protective membrane on the metal surface, therefore, the corrosion resistance of metal was improved. However, two different equivalent circuits were obtained for the constructed coatings due to their distinct surface roughness (Cui et al., 2017). The integral composition of pure WPA coating, sample I and sample II were uniform, and the surface of them were smooth. But sample III, sample IV and sample V had rough surface because BTA@ZnO MCs were distributed on the top of the coating. Thus, circuit A was suitable for pure WPA coating, sample I and sample II. Circuit B was appropriate for sample III, sample IV and sample V.

Based on the above fitting circuits, the corresponding electrochemical corrosion parameters of different coatings were obtained as shown in Table 2. Since the corrosive medium was the same, the fitted R_s values of all coating systems were basically unchanged. The fitted R_c values of the five composite coating systems were all higher than that of pure WPA coating and also showed a growth trend in the following order: $I < IV < V < II < III$. This suggested that the coating system III had the best corrosion protection ability to the substrate. The C_c value of coating system II and the Q_c value of coating system III were much lower than that of other coating systems, meaning the better densities of coating systems II and III. Compared to the coating systems I and II obtained by the hybrid method, the coating systems III, IV, and V fabricated by the layer-by-layer spraying method had higher R_{ox}/R_{ct} val-

ues. These results indicated that more BTA was released from the microcapsules in the coatings fabricated by the layer-by-layer spraying method and reacted with the metal substrate to form a corrosion resistant protective layer. While in the hybrid method, the release amount of BTA was limited since the microcapsules were wrapped by the polymer chains. In addition, the Q_{ox} and Q_{dl} of the coating system III were the smallest compared with other coating systems, further revealing the best compactness and BTA release in coating system III. Overall, coating system III possessed the best protective effect for metal.

In order to clarify the impact of aziridine cross-linker and BTA@ZnO MCs on the corrosion resistance, the surface morphology, structure and hydrophobicity of pure WPA coating and five composite coating systems were investigated by SEM, FTIR and contact angle tests. The BTA@ZnO MCs used in this work are rod-like spindle structures with diameters ranging from 30 nm to 100 nm and lengths of 200 nm to 800 nm. And there are also flower-like BTA@ZnO MCs composed of these rod-like spindles (Bao et al., 2019). As shown in Fig. 3A and B, it could be seen that the introduction of BTA@ZnO MCs increased the contact angle of the coating. This was because the hydroxyl groups and Zn^{2+} on the surface of BTA@ZnO MCs could interact with the carboxyl groups on the polyacrylate chain, thereby reducing the number of exposed hydrophilic groups in the coating. From the SEM images in Fig. 3B and C, some micro-nano pores were observed on coating system I, while coating system II showed a relatively dense surface. What's more, the FT-IR spectra (Fig. 4) of the coating systems also showed a novel peak at 1737 cm^{-1} after introducing the aziridine crosslinker. It should be ascribed to $\text{C}=\text{O}$ stretching vibration in saturated car-

Table 2 Electrochemical impedance parameters of the pure WPA coating and different composite coating systems in 3.5 wt% NaCl solution.

Coating system	R_s ($\Omega\text{ cm}^2$)	C_c or Q_c (F cm^{-2})	n	R_c ($\Omega\text{ cm}^2$)	Q_{ox} (F cm^{-2})	n	R_{ox} ($\Omega\text{ cm}^2$)	C_{dl} or Q_{dl} (F cm^{-2})	n	R_{ct} ($\Omega\text{ cm}^2$)
Blank	4.078	1.024×10^{-5}	—	307.6	2.293×10^{-3}	0.756	43.50	1.412×10^{-3}	0.606	4.713
I	3.931	1.287×10^{-5}	—	676.3	4.902×10^{-4}	0.767	12.15	6.186×10^{-5}	0.805	10.16
II	1.418	5.868×10^{-6}	—	1272	4.886×10^{-4}	0.690	44.60	2.157×10^{-4}	0.692	7.028
III	7.218	7.732×10^{-6}	0.880	1816	3.197×10^{-5}	0.743	1050	2.073×10^{-5}	—	3068
IV	3.927	1.896×10^{-4}	0.821	738.3	3.695×10^{-4}	0.773	114.8	2.572×10^{-4}	—	1032
V	4.233	4.151×10^{-5}	0.779	925.2	2.458×10^{-4}	0.692	321.4	8.794×10^{-5}	—	2497

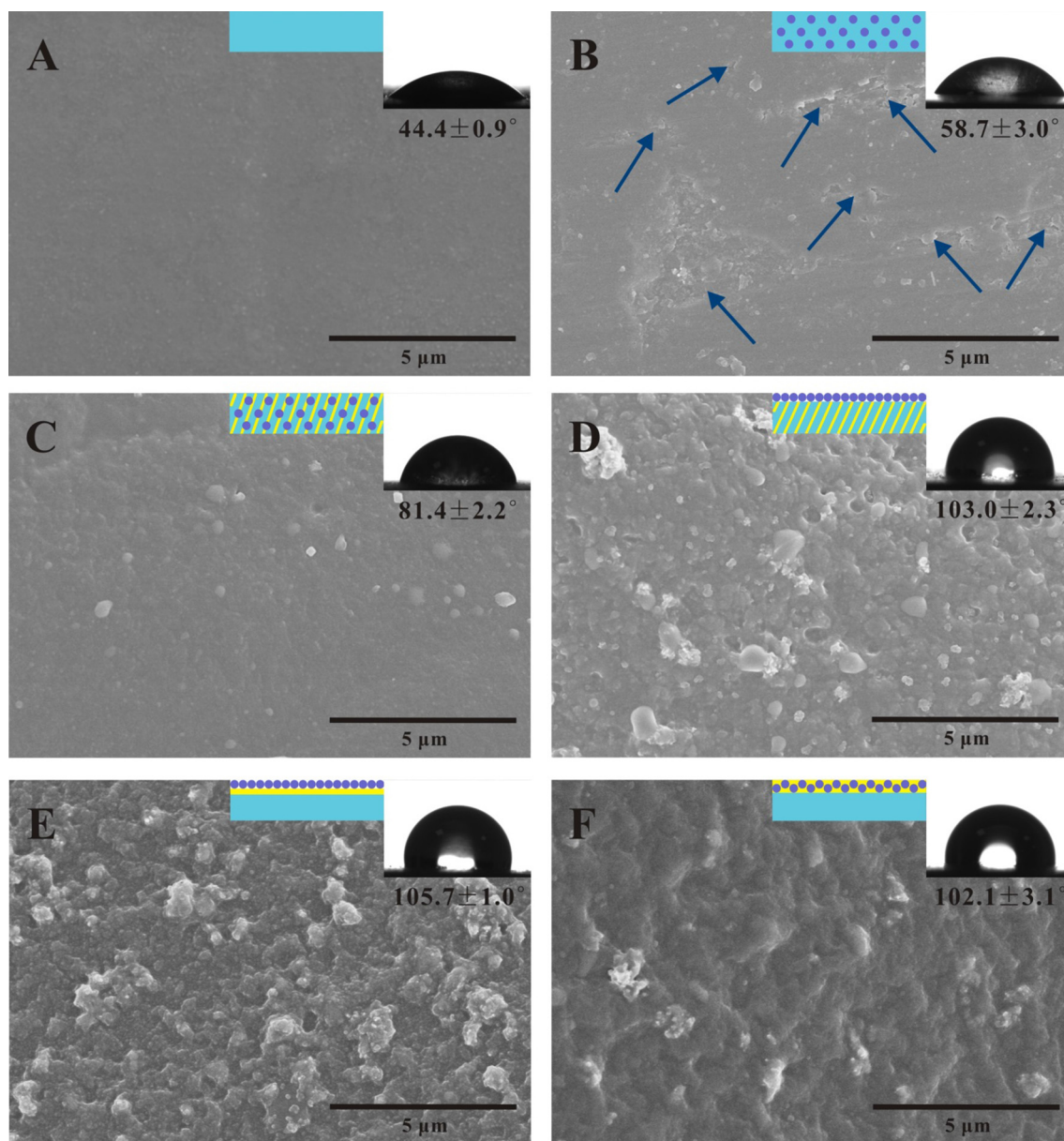


Fig. 3 SEM images and water contact angles of the pure WPA coating (A), composite coating systems I (B), II (C), III (D), IV (E) and V (F). (Micro-nano pores were observed at the direction of the blue arrows.)

boxylic ester (Li and Tang, 2016), implying the cross-linking reaction between the aziridine ring and the carboxyl group. These results indicated that the introduction of aziridine cross-linker greatly improved the compactness of the coating and less corrosive molecules could penetrate into the coating, thereby revealing higher R_c and lower C_c values. Besides, the water contact angle of the coating increased from $\sim 58.7^\circ$ to $\sim 81.4^\circ$ after introducing aziridine cross-linker. This implied that the addition of aziridine cross-linker also improved the hydrophobicity of the coating. Fig. 3D–F displayed the surface morphologies and water contact angles of coating systems III, IV and V. SEM images showed that the surfaces of these layered coating systems were rougher than hybrid coating systems. In addition, their water contact angle was increased by $\sim 20^\circ$ relative to the hybrid coating system II. These findings suggested that the surface roughness of the coating was

increased when the BTA@ZnO MCs were distributed on the top of the coating and the feeding mode of the aziridine cross-linker had little effect on the surface roughness of the coating. It is understandable because the distribution of the microcapsules on top of the coating resulted in the formation of microstructures. Clearly, the position of BTA@ZnO MCs in the coating played an important role in the hydrophobicity of the composite coating. In fact, some studies have shown that the improvement in hydrophobicity of the coating could provide sufficient corrosion protection for the substrate by extending the penetration time of the corrosive medium (Lu et al., 2017). Therefore, coating system III exhibited better performances than other composite coating systems in improving corrosion resistance due to its superior barrier properties and hydrophobicity. However, it should be noted that the feeding mode of aziridine cross-linker was also quite important. When

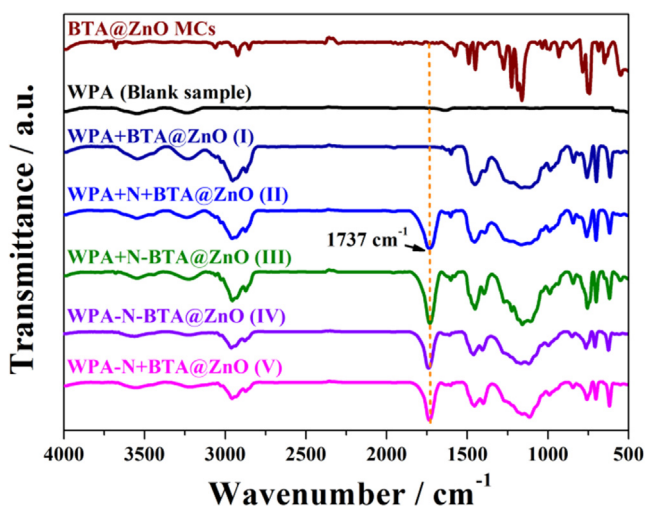


Fig. 4 FT-IR spectra of the BTA@ZnO MCs, pure WPA coating and five composite coating systems.

the aziridine cross-linker was applied separately from the polyacrylate emulsion (i.e. coating system IV and V), the improvements in corrosion resistance of the coating were not significant. It could be attributed to the decreasing cross-linking density of the polymeric matrix when the cross-linking reaction occurred after the film-forming (He et al., 2011). Similarly, the reason for the different results of the coating systems IV and V could also be ascribed to the degree of cross-linking. When the cross-linker was fed together with the microcapsules (i.e. coating system V), the composite coating had higher corrosion resistance. Considering the potential of coating system III to improve the corrosion resistance of coatings, the effects of the amount of aziridine cross-linker and BTA@ZnO MCs on the coating properties were further investigated.

3.2. Influence of aziridine cross-linker amount

Different amounts of aziridine cross-linker were uniformly introduced into WPA to fabricate coating system III. Fig. 5 showed the Nyquist and Bode-impedance plots of these coatings immersed in 3.5 wt% NaCl aqueous solution. As the amount of aziridine cross-linker increased from 1 mg/cm² to 7 mg/cm², the capacitive arc diameter and $|Z|_{0.01 \text{ Hz}}$ value of the coating increased significantly. These results illustrated that the amount of aziridine cross-linker had a profound effect on the corrosion resistance of the coating. In the initial amount range from 1 mg/cm² to 3 mg/cm², the capacitive arc diameter and $|Z|_{0.01 \text{ Hz}}$ value increased slowly, indicating that an integrated network has not yet been formed. During the increase in amount of aziridine cross-linker from 3 mg/cm² to 5 mg/cm², a significant increase in the capacitive arc diameter and $|Z|_{0.01 \text{ Hz}}$ value was observed. This apparent shift may be due to the fact that 5 mg/cm² of aziridine cross-linker was sufficiently high to form an integrated network and thus the coating became continuous and intact. As shown in Fig. 5C, the phase angle plot showed two time constants. The time constant appeared at high frequency range could be attributed to the coating layer, while the time constant at low frequency range was corresponding to a corrosion process taking place at the metal/coating interface (Li et al., 2016). When the amount of

aziridine cross-linker was increased from 3 mg/cm² to 5 mg/cm², the phase angle increased dramatically. It suggested that the barrier properties of the coating were greatly improved and the corrosion reaction at the metal/coating interface was rapidly reduced. When the amount of aziridine cross-linker was further increased to 7 mg/cm², the corrosion resistance of the coating was slightly improved. It implied that the amount of the aziridine cross-linker introduced into the polyacrylate matrix tends to be saturated. In addition, further experiments revealed that excessive addition of aziridine cross-linker (> 7 mg/cm²) affected the flowability of the polyacrylate emulsion due to rapid cross-linking of the polyacrylate chains. It would reduce the uniformity of the final coating tremendously and even affect spraying operations. These above analyses confirmed that coating system III had the best corrosion resistance when the amount of the aziridine cross-linker was 7 mg/cm².

Afterwards, the adhesion of the coatings with different amounts of aziridine cross-linker on the surface of the substrate was measured using a cross-cut test according to standard method, ISO 2409: 2013E. Measured adhesion of these coatings was all grade 0 because the introduction of aziridine cross-linker in WPA maintained the excellent adhesion between the coating and the substrate. Fig. 6A displayed the effect of the amount of aziridine cross-linker on the surface properties of these coatings, i.e. pencil hardness and water contact angle. With the increase of aziridine cross-linker amount, the pencil hardness of the coating increased slightly from 3H to 4H. It proved that the aziridine cross-linker improved the firmness of the coating, which was consistent with previous reports (He et al., 2011). However, the water contact angle of these coatings produced only minor variations, indicating that the amount of aziridine cross-linker did not contribute to the hydrophobicity of the coating. Furthermore, the water absorption of these coatings with different amounts of aziridine cross-linker were studied. As shown in Fig. 6B, their water absorption decreased gradually as the amount of the aziridine cross-linker increased. It implied that the barrier properties of the coating was greatly improved by introducing more aziridine cross-linkers, since aziridine groups could react with the carboxyl and hydroxyl groups in polyacrylate chains (Fig. 10) and form network structures (He et al., 2011; Liu and Ke, 2011). Consequently, a coating containing 7 mg/cm² of aziridine cross-linker was selected as an optimized sample to further explore the effect of the amount of BTA@ZnO MCs on the coating properties.

3.3. Influence of BTA@ZnO MCs amount

The impedance spectra of coatings with different amounts of BTA@ZnO MCs immersed in 3.5 wt% NaCl aqueous solution were represented in the form of Nyquist and Bode plots in Fig. 7. A significant improvement in the corrosion resistance of the coating was observed when the BTA@ZnO MCs amount was increased from 0.8 mg/cm² to 2.5 mg/cm². Instead, as the amount of BTA@ZnO MCs further increased to 4.2 mg/cm², the corrosion resistance of the coating decreased slightly. Obviously, the highest absolute impedance values in all frequency ranges were obtained for the coating with 2.5 mg/cm² of BTA@ZnO MCs. Its $|Z|_{0.01 \text{ Hz}}$ value reached $6.11 \times 10^5 \Omega \cdot \text{cm}^2$, which was not as good as the cor-

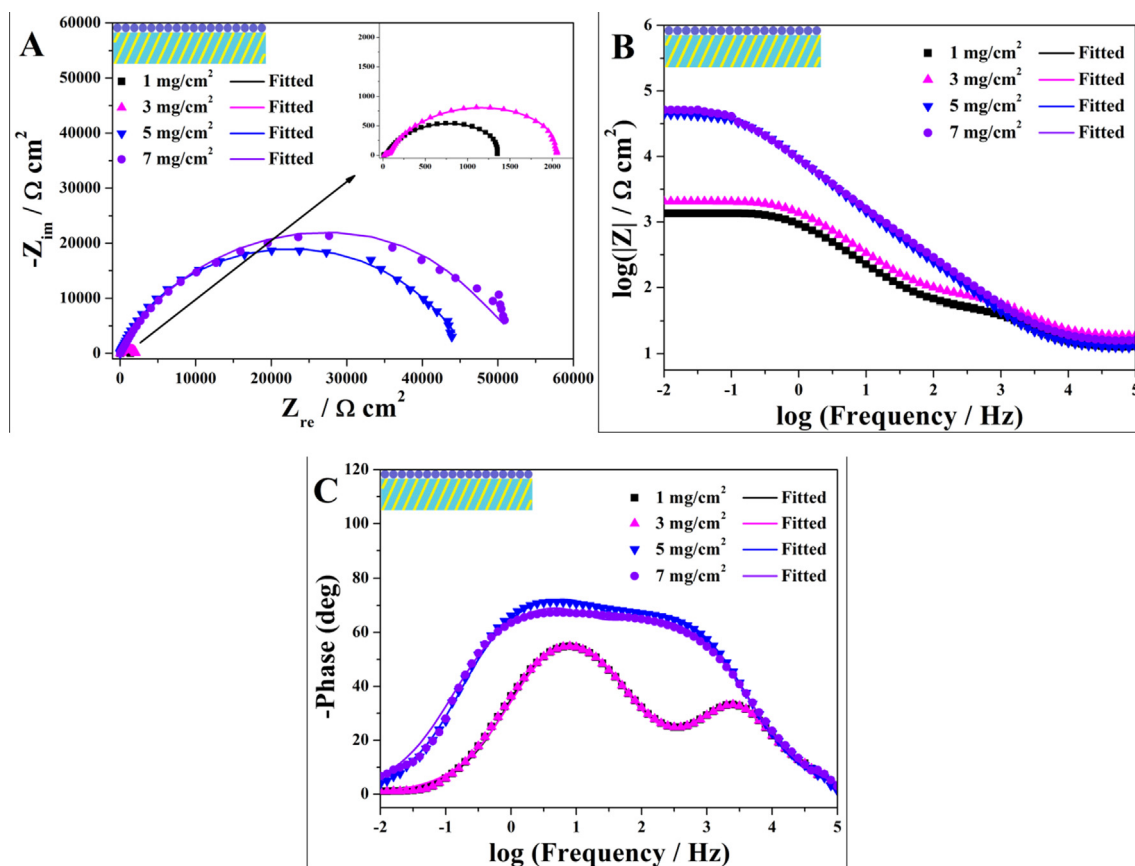


Fig. 5 Electrochemical impedance spectroscopy of coating system III with different aziridine cross-linker amounts immersed in 3.5 wt% NaCl aqueous solution. Nyquist plots (A), Bode plots (B and C).

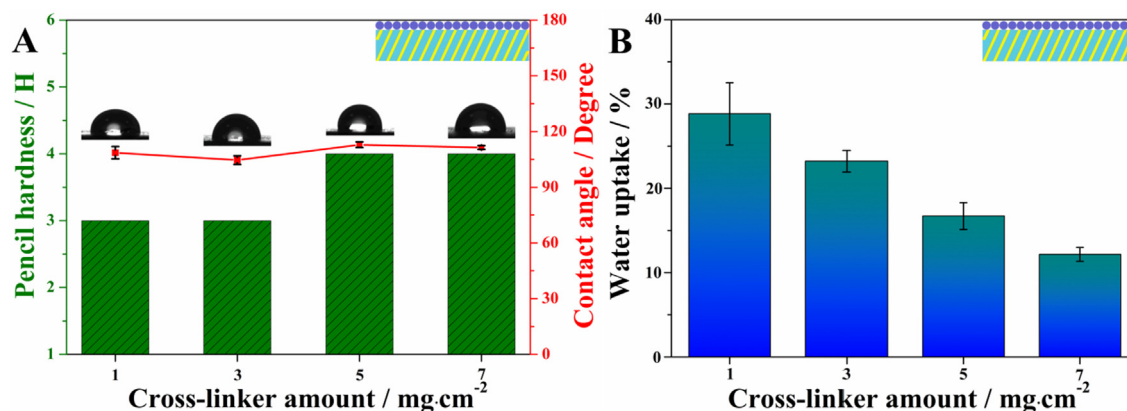


Fig. 6 (A) Pencil hardness and water contact angles, (B) water absorption rates of coating system III with different aziridine cross-linker amounts.

rosion resistance ($10^{8-9} \Omega \text{ cm}^2$) of waterborne epoxy coatings (Liu et al., 2018a,b; Cui et al., 2018), but higher than the existing waterborne polyacrylate coatings ($10^{2-3} \Omega \text{ cm}^2$) (Gao et al., 2020; Song et al., 2017).

In order to understand the relationship between corrosion resistance and the amount of BTA@ZnO MCs, the surface properties of these coatings were tested. As shown in Fig. 8A, the pencil hardness of the coating was maintained at 4H, while the water contact angle of the coating showed a larger increase with the amount of BTA@ZnO MCs from

0.8 to 2.5 mg/cm². When the amount of BTA@ZnO MCs was 2.5 and 4.2 mg/cm², the water contact angle of the coating reached above 150°, indicating that the coating surfaces was superhydrophobic, thus enhancing the barrier properties of the coating (Yang et al., 2017). These findings agreed well with the EIS analysis, indicating that the corrosion resistance of the coating was highly dependent on its surface hydrophobicity. To examine the formation of superhydrophobic surfaces, SEM and AFM images of coatings with 0.8 mg/cm² and 2.5 mg/cm² of BTA@ZnO MCs were obtained as shown in

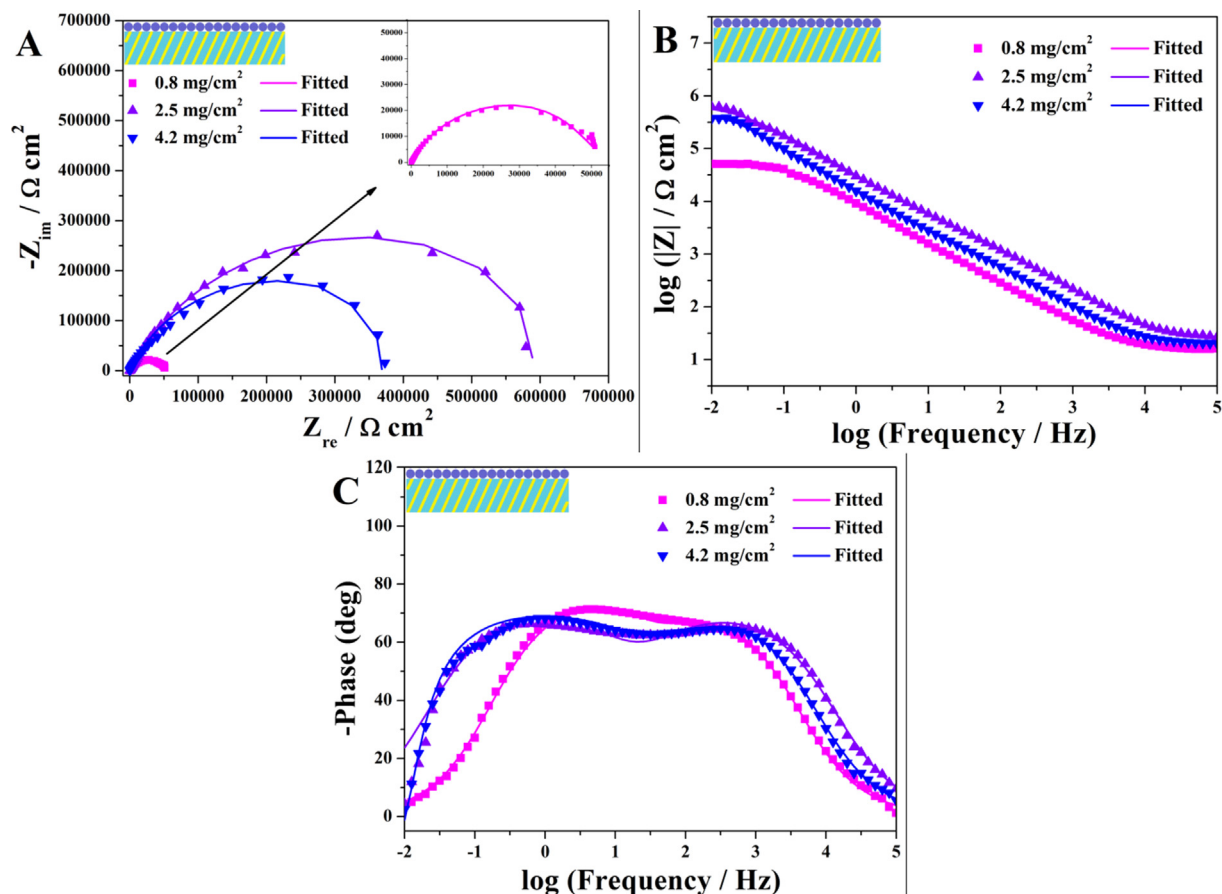


Fig. 7 Electrochemical impedance spectroscopy of coating system III with different BTA@ZnO MCs amounts immersed in 3.5 wt% NaCl aqueous solution. Nyquist plots (A), Bode plots (B and C).

Fig. 8B and C, respectively. Compared with the former ($R_a = 100$ nm), the latter displayed a continuous roughness close to the micron level ($R_a = 800$ nm). This microstructure helped to protect the substrate from corrosion attack (Li et al., 2015; Wang and Gong, 2017). Therefore, the effect of the amount of BTA@ZnO MCs on the corrosion resistance of the coating was mainly caused by the roughness formed by micro-nano materials. From the inset optical images (collecting a drop of water on the coating) in the Fig. 8A, the surface of the coatings with higher BTA@ZnO MCs amounts (2.5 and 4.2 mg/cm²) was highly hydrophobic. However, $|Z|_{0.01 \text{ Hz}}$ decreased slightly with increasing BTA@ZnO MCs amount from 2.5 to 4.2 mg/cm². It could attribute to poor adhesion between the excess BTA@ZnO MCs and the polyacrylate matrix. This was proved by the adhesion test. More microcapsules were dropped from the coating during cross-cut test when overmuch BTA@ZnO MCs (4.2 mg/cm²) was introduced into the coating system III. This is because polyacrylate chains and crosslinkers could not capture BTA@ZnO MCs in the outermost coating, thereby destroying the integrity of the entire coating.

3.4. Salt spray exposure tests

To further examine the corrosion behaviour of the optimized coating system III (7 mg/cm² of aziridine cross-linker,

2.5 mg/cm² of BTA@ZnO MCs), a total of 5 h of salt spray exposure tests were performed. Here, the coating system I served as a reference sample. Their appearances after salt spray exposure test were shown in Fig. 9. As the exposure time prolonged, corrosion occurred over the entire surface of the coating system I. While for coating system III, corrosion products were mainly accumulated in the scratch area. These results effectively proved the superiority of the layer-by-layer spraying method in building anti-corrosive coatings. The reasons can be concluded the following two aspects: (i) a highly cross-linked network structure formed by polyacrylate chains and aziridine cross-linkers; (ii) a sufficient surface roughness constructed by anti-corrosive micro-nano materials.

3.5. Corrosion protection mechanism

Based on the above analysis, the possible corrosion protection mechanism of coating system III was described in Fig. 10. When the coating is exposure to a corrosive environment, the superhydrophobic surface provided by BTA@ZnO MCs firstly avoids rapid erosion of corrosive species. As the corrosion time prolongs, the corrosion resistance of the coating mainly depends on the chemical cross-linking between the aziridine cross-linker and the polyacrylate chain (Bahlakeh et al., 2017). A sufficient amount of aziridine cross-linker can enhance the integrity and compactness of the coating. Mean-

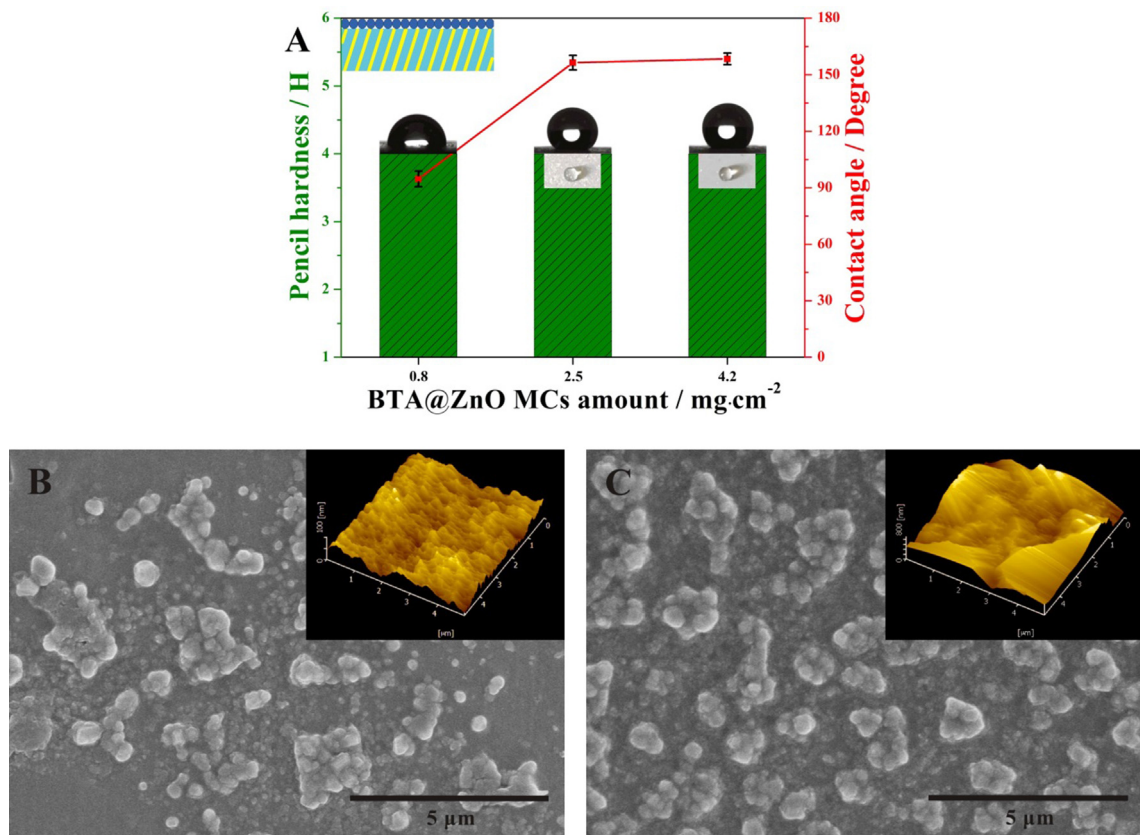


Fig. 8 (A) Pencil hardness and water contact angles of coating system III with different BTA@ZnO MCs amounts (inset: optical images of a drop of water on the coating), SEM and AFM images of coating system III with (B) $0.8 \text{ mg}/\text{cm}^2$ and (C) $2.5 \text{ mg}/\text{cm}^2$ of BTA@ZnO MCs.

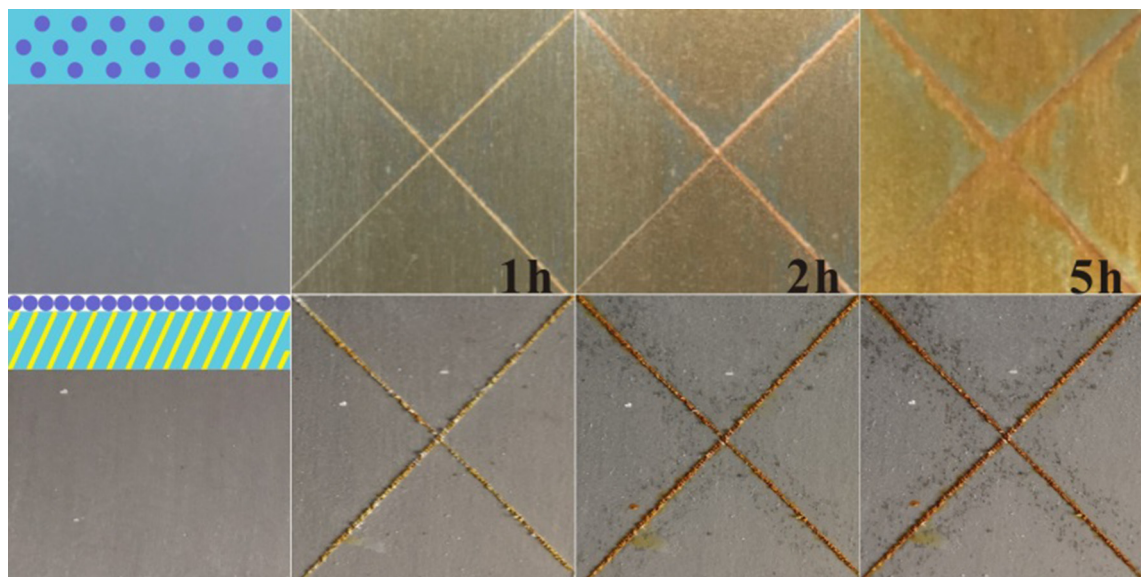


Fig. 9 Images of the salt spray-tested tinplates coated with coating systems I (top) and III (bottom).

while, partial BTA@ZnO MCs existed in the coating can act as a barrier protective filler to fill the pores of the coating (Mostafaei and Nasirpour, 2013; Sonawane et al., 2010). The hydroxyl groups and Zn^{2+} on the surface of BTA@ZnO MCs can chemically interact (i.e. hydrogen bondings and elec-

trostatic interaction) with the polar groups of the polyacrylate chains (Ramezanzadeh et al., 2019). Such highly cross-linked and dense structure greatly hinders the penetration of water, chlorides, and other corrosive media oriented to the vertical direction in the coating's thickness. Once the continuous pen-

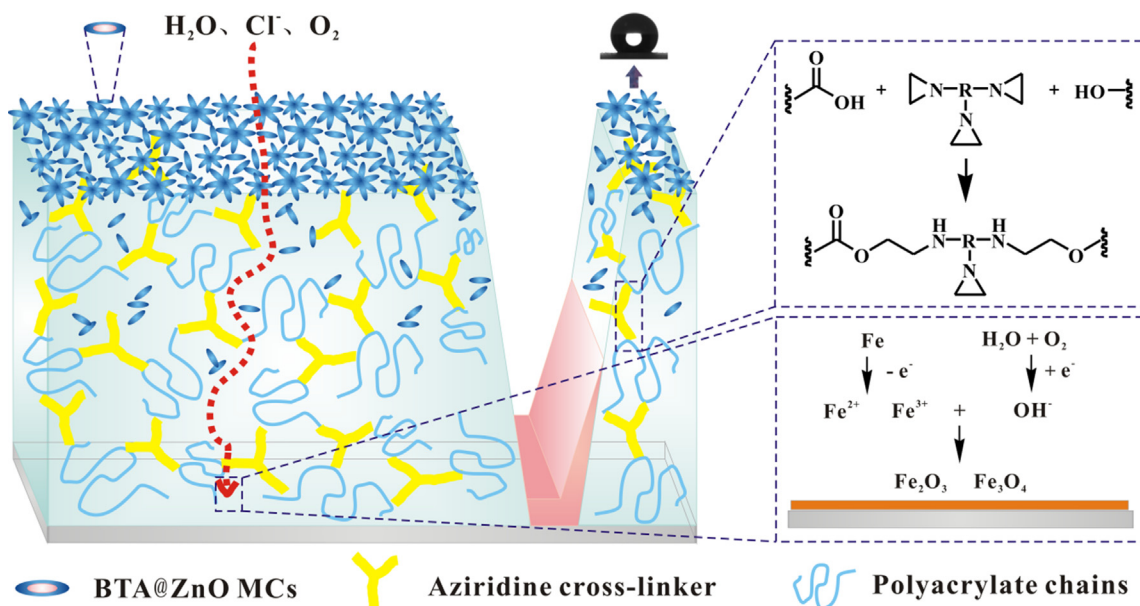


Fig. 10 The possible corrosion protective mechanism of coating system III.

etration of corrosive medium is happened, the BTA is gradually released from the microcapsules. The released BTA with nitrogen heteroatoms shares their electrons with unoccupied orbitals of surface metal atoms and form a protective membrane on the metal surface (Tamil Selvi et al., 2003; Popova and Christov, 2006). In addition, when the corrosive medium is in contact with the metal surface, the corrosion reaction occurs on the metal surface. The Fe ions (Fe^{2+} and Fe^{3+}) generated by the dissolution of the metal are converted into passivated Fe_2O_3 and Fe_3O_4 to protect the substrate (Radhakrishnan et al., 2009).

4. Conclusions

In this paper, a layer-by-layer assembled technology for constructing anti-corrosive coatings was proposed. Firstly, five types of WPA composite coating systems were designed according to the feeding mode of aziridine cross-linker and the position of BTA@ZnO MCs. EIS and electrical equivalent circuits were used to evaluate the corrosion resistance of these composite coating systems and analyze their electrochemical processes. By spraying the mixture of WPA and aziridine crosslinker as the bottom layer and BTA@ZnO MCs as the top layer, the resulting composite coating exhibited higher corrosion resistance and hydrophobic properties. Subsequently, studies on the EIS and physical properties of the coating system revealed that the amounts of aziridine cross-linker and BTA@ZnO MCs had significant contributions in improving its barrier property and hydrophobicity. Upon the amounts of aziridine cross-linker and BTA@ZnO MCs were 7 mg/cm^2 and 2.5 mg/cm^2 , respectively, the $|Z|_{0.01\text{Hz}}$ value of coating system III was $6.11 \times 10^5 \Omega\text{-cm}^2$, higher than that of the bare sample ($2.63 \times 10^2 \Omega\text{-cm}^2$) by three orders of magnitude. The salt spray exposure test also proved the superiority of this layer-by-layer assembly technology in constructing anti-corrosive coatings. The corrosion protection mechanism was mainly based on the following two aspects: (i) a highly cross-

linked network structure formed by polymer matrix and cross-linkers; (ii) a sufficient surface roughness constructed by anti-corrosive micro-nano materials.

Declaration of Competing Interest

The authors declare that they have no known competing financial interests or personal relationships that could have appeared to influence the work reported in this paper.

Acknowledgements

This work was supported by the financial support of the National Natural Science Foundation of China (No. 21878181) and the Key Research and Development Program of Shaanxi Province (No. 2018ZDXM-GY-118).

References

- Bahlakeh, G., Ramezanzadeh, B., Ramezanzadeh, M., 2017. Corrosion protective and adhesion properties of a melamine-cured polyester coating applied on steel substrate treated by a nanostructure cerium-lanthanum film. *J. Taiwan Inst. Chem. Eng.* 81, 419–434. <https://doi.org/10.1016/j.jtice.2017.09.033>.
- Bao, Y., Chen, Y., 2018. Effect of functional monomers on the corrosion resistance of polyacrylate latex film. *Polym. Mater. Sci. Eng.* 34, 75–80.
- Bao, Y., Yan, Y., Chen, Y., Ma, J., Zhang, W., Liu, C., 2019. Facile fabrication of BTA@ZnO microcapsules and their corrosion protective application in waterborne polyacrylate coatings. *Prog. Org. Coat.* 136, 105233. <https://doi.org/10.1016/j.porgcoat.2019.105233>.
- Chen, T., Fu, JiaJun, 2012. An intelligent anticorrosion coating based on pH-responsive supramolecular nanocontainers. *Nanotechnology* 23 (50), 505705. <https://doi.org/10.1088/0957-4484/23/50/505705>.
- Chen, T., Chen, R., Jin, Z., Liu, J., 2015. Engineering hollow mesoporous silica nanocontainers with molecular switches for

- continuous self-healing anticorrosion coating. *J. Mater. Chem. A* 3 (18), 9510–9516. <https://doi.org/10.1039/C5TA01188D>.
- Christopher, G., Anbu Kulandainathan, M., Harichandran, G., 2015. Highly dispersive waterborne polyurethane/ZnO nanocomposites for corrosion protection. *J. Coat. Technol. Res.* 12 (4), 657–667. <https://doi.org/10.1007/s11998-015-9674-3>.
- Cui, M., Ren, S., Xue, Q., Zhao, H., Wang, L., 2017. Carbon dots as new eco-friendly and effective corrosion inhibitor. *J. Alloys Compd.* 726, 680–692. <https://doi.org/10.1016/j.jallcom.2017.08.027>.
- Cui, M., Ren, S., Zhao, H., Xue, Q., Wang, L., 2018. Polydopamine coated graphene oxide for anticorrosive reinforcement of waterborne epoxy coating. *Chem. Eng. J.* 335, 255–266. <https://doi.org/10.1016/j.cej.2017.10.172>.
- Fu, C.e., Qin, H.-W., Ben, H.-J., Han, J., Cui, W.-Z., Cheng, F.a., Chen, Y.u., 2014. Acrylate-vinylidene chloride copolymers derived from corresponding water-borne latexes: Influence of acrylate units on their potential as heavy-duty anticorrosive coating materials. *J. Appl. Polym. Sci.* 131 (8). <https://doi.org/10.1002/app.40192>.
- Gao, F., Du, A.n., Ma, R., Lv, C., Yang, H., Fan, Y., Zhao, X., Wu, J., Cao, X., 2020. Improved corrosion resistance of acrylic coatings prepared with modified MoS₂ nanosheets. *Colloids Surf., A* 587, 124318. <https://doi.org/10.1016/j.colsurfa.2019.124318>.
- Grundmeier, G., Schmidt, W., Stratmann, M., 2000. Corrosion protection by organic coatings: electrochemical mechanism and novel methods of investigation. *Electrochim. Acta* 45 (15-16), 2515–2533. [https://doi.org/10.1016/S0013-4686\(00\)00348-0](https://doi.org/10.1016/S0013-4686(00)00348-0).
- He, M., Zhang, Q.Y., Guo, J.Y., 2011. Synthesis and characterization of water based acrylic pressure sensitive adhesive of surface protection tape. *Adv. Mater. Res.* 306-307, 1785–1791. <https://doi.org/10.4028/www.scientific.net/AMR.306-307.1785>.
- Javadi, E., Ghaffari, M., Bahlakeh, G., Taheri, P., 2019. Photocatalytic, corrosion protection and adhesion properties of acrylic nanocomposite coating containing silane treated nano zinc oxide: A combined experimental and simulation study. *Prog. Org. Coat.* 135, 496–509. <https://doi.org/10.1016/j.porgcoat.2019.06.039>.
- Li, J., Wu, R., Jing, Z., Yan, L., Zha, F., Lei, Z., 2015. One-step spray-coating process for the fabrication of colorful superhydrophobic coatings with excellent corrosion resistance. *Langmuir* 31 (39), 10702–10707. <https://doi.org/10.1021/acs.langmuir.5b02734>.
- Li, J., Cui, J., Yang, J., Li, Y., Qiu, H., Yang, J., 2016. Reinforcement of graphene and its derivatives on the anticorrosive properties of waterborne polyurethane coatings. *Compos. Sci. Technol.* 129, 30–37. <https://doi.org/10.1016/j.compscitech.2016.04.017>.
- Li, X.-Q., Tang, R.-C., 2016. Crosslinked and Dyed Chitosan Fiber Presenting Enhanced Acid Resistance and Bioactivities. *Polymers* 8 (4), 119. <https://doi.org/10.3390/polym8040119>.
- Liang, J., Wu, X.-W., Ling, Y., Yu, S., Zhang, Z., 2018. Trilaminar structure hydrophobic graphene oxide decorated organosilane composite coatings for corrosion protection. *Surf. Coat. Technol.* 339, 65–77. <https://doi.org/10.1016/j.surfcoat.2018.02.002>.
- Liu, F.F., Ke, T.H., 2011. Preliminary studies on washing durability of fire-retardant viscose fiber. *Adv. Mater. Res.* 287-290, 2598–2601. <https://doi.org/10.4028/www.scientific.net/AMR.287-290.2598>.
- Liu, C., Qiu, S., Du, P., Zhao, H., Wang, L., 2018a. An ionic liquid-graphene oxide hybrid nanomaterial: synthesis and anticorrosive applications. *Nanoscale* 10 (17), 8115–8124. <https://doi.org/10.1039/C8NR01890A>.
- Liu, C., Du, P., Nan, F., Zhao, H., Wang, L., 2018b. Dual functions of imidazole-based polymeric ionic liquid (PIL) on the anticorrosive performance of graphene-based waterborne epoxy coatings. *Surf. Topogr.: Metrol. Prop.* 6 (2), 024004. <https://doi.org/10.1088/2051-672X/aab587>.
- Lu, H., Zhang, S., Li, W., Cui, Y., Yang, T., 2017. Synthesis of graphene oxide-based sulfonated oligoanilines coatings for synergistically enhanced corrosion protection in 3.5% NaCl solution. *ACS Appl. Mater. Interfaces* 9 (4), 4034–4043. <https://doi.org/10.1021/acsami.6b13722>.
- Malucelli, G., Alongi, J., Gioffredi, E., Lazzari, M., 2013. Thermal, rheological, and barrier properties of waterborne acrylic nanocomposite coatings based on boehmite or organo-modified montmorillonite. *J. Therm. Anal. Calorim.* 111 (2), 1303–1310. <https://doi.org/10.1007/s10973-012-2510-4>.
- Mihelčič, M., Gaberšček, M., Di Carlo, G., Giuliani, C., Salzano de Luna, M., Lavorgna, M., Surca, A.K., 2019. Influence of silsesquioxane addition on polyurethane-based protective coatings for bronze surfaces. *Appl. Surf. Sci.* 467–468, 912–925. <https://doi.org/10.1016/j.apsusc.2018.10.217>.
- Mostafaei, A., Nasirpour, F., 2013. Electrochemical study of epoxy coating containing novel conducting nanocomposite comprising polyaniline-ZnO nanorods on low carbon steel. *Corros. Eng., Sci. Technol.* 48 (7), 513–524. <https://doi.org/10.1179/1743278213Y.0000000084>.
- Nardeli, J.V., Fugivara, C.S., Taryba, M., Montemor, M.F., Ribeiro, S.J.L., Benedetti, A.V., 2020. Novel healing coatings based on natural-derived polyurethane modified with tannins for corrosion protection of AA2024-T3. *Corros. Sci.* 162, 108213. <https://doi.org/10.1016/j.corsci.2019.108213>.
- Park, J.H., Park, J.M., 2014. Electrophoretic deposition of graphene oxide on mild carbon steel for anti-corrosion application. *Surf. Coat. Technol.* 254, 167–174. <https://doi.org/10.1016/j.surfcoat.2014.06.007>.
- Popova, A., Christov, M., 2006. Evaluation of impedance measurements on mild steel corrosion in acid media in the presence of heterocyclic compounds. *Corros. Sci.* 48 (10), 3208–3221. <https://doi.org/10.1016/j.corsci.2005.11.001>.
- Radhakrishnan, S., Sonawane, N., Siju, C.R., 2009. Epoxy powder coatings containing polyaniline for enhanced corrosion protection. *Prog. Org. Coat.* 64 (4), 383–386. <https://doi.org/10.1016/j.porgcoat.2008.07.024>.
- Ramezanzadeh, M., Bahlakeh, G., Sanaei, Z., Ramezanzadeh, B., 2019. Interfacial adhesion and corrosion protection properties improvement of a polyester-melamine coating by deposition of a novel green praseodymium oxide nanofilm: A comprehensive experimental and computational study. *J. Ind. Eng. Chem.* 74, 26–40. <https://doi.org/10.1016/j.jiec.2019.01.037>.
- Shi, H., Liu, F., Han, E., 2010. Corrosion behaviour of sol-gel coatings doped with cerium salts on 2024-T3 aluminum alloy. *Mater. Chem. Phys.* 124 (1), 291–297. <https://doi.org/10.1016/j.matchemphys.2010.06.035>.
- Sonawane, S.H., Teo, B.M., Brotchie, A., Grieser, F., Ashokkumar, M., 2010. Sonochemical synthesis of ZnO encapsulated functional nanolatex and its anticorrosive performance. *Ind. Eng. Chem. Res.* 49 (5), 2200–2205. <https://doi.org/10.1021/ie9015039>.
- Song, D., Yin, Z., Liu, F., Wan, H., Gao, J., Zhang, D., Li, X., 2017. Effect of carbon nanotubes on the corrosion resistance of waterborne acrylic coatings. *Prog. Org. Coat.* 110, 182–186. <https://doi.org/10.1016/j.porgcoat.2017.04.043>.
- Tamil Selvi, S., Raman, V., Rajendran, N., 2003. Corrosion inhibition of mild steel by benzotriazole derivatives in acidic medium. *J. Appl. Electrochem.* 33 (12), 1175–1182. <https://doi.org/10.1023/B:JACH.0000003852.38068.3f>.
- Tian, W., Meng, F., Liu, L.i., Li, Y., Wang, F., 2015. The failure behaviour of a commercial highly pigmented epoxy coating under marine alternating hydrostatic pressure. *Prog. Org. Coat.* 82, 101–112. <https://doi.org/10.1016/j.porgcoat.2015.01.009>.
- Wang, Y., Gong, X., 2017. Superhydrophobic coatings with periodic ring structured patterns for self-cleaning and oil-water separation. *Adv. Mater. Interfaces* 4 (16), 1700190. <https://doi.org/10.1002/admi.201700190>.
- Xia, Y., Larock, R.C., 2011. Castor-oil-based waterborne polyurethane dispersions cured with an aziridine-based crosslinker. *Macromol. Mater. Eng.* 296 (8), 703–709. <https://doi.org/10.1002/mame.201000431>.
- Xia, Y., He, Y.i., Chen, C., Wu, Y., Chen, J., 2019. MoS₂ nanosheets modified SiO₂ to enhance the anticorrosive and mechanical

- performance of epoxy coating. *Prog. Org. Coat.* 132, 316–327. <https://doi.org/10.1016/j.porgcoat.2019.04.002>.
- Yang, Z., Wang, L., Sun, W., Li, S., Zhu, T., Liu, W., Liu, G., 2017. Superhydrophobic epoxy coating modified by fluorographene used for anti-corrosion and self-cleaning. *Appl. Surf. Sci.* 401, 146–155. <https://doi.org/10.1016/j.apsusc.2017.01.009>.
- Yao, M., Tang, E., Guo, C., Liu, S., Tian, H., Gao, H., 2017. Synthesis of waterborne epoxy/polyacrylate composites via miniemulsion polymerization and corrosion resistance of coatings. *Prog. Org. Coat.* 113, 143–150. <https://doi.org/10.1016/j.porgcoat.2017.09.008>.
- Ye, X., Wang, Z., Ma, L., Wang, Q., Chu, A., 2019. Zinc oxide array/polyurethane nanocomposite coating: Fabrication, characterization and corrosion resistance. *Surf. Coat. Technol.* 358, 497–504. <https://doi.org/10.1016/j.surfcoat.2018.11.080>.
- Ye, Y., Zhang, D., Liu, Z., Liu, W., Zhao, H., Wang, L., Li, X., 2018. Anti-corrosion properties of oligoaniline modified silica hybrid coatings for low-carbon steel. *Synth. Met.* 235, 61–70. <https://doi.org/10.1016/j.synthmet.2017.11.015>.
- Zhang, M.Q., Rong, M.Z., Yu, S.L., Wetzel, B., Friedrich, K., 2002. Improvement of tribological performance of epoxy by the addition of irradiation grafted nano-inorganic particles. *Macromol. Mater. Eng.* 287 (2), 111–115. [https://doi.org/10.1002/1439-2054\(20020201\)287:2<111::AID-MAME111>3.0.CO;2-I](https://doi.org/10.1002/1439-2054(20020201)287:2<111::AID-MAME111>3.0.CO;2-I).
- Zhang, J., Yang, Y., Lou, J., 2016. Investigation of hexagonal boron nitride as an atomically thin corrosion passivation coating in aqueous solution. *Nanotechnology* 27 (36), 364004. <https://doi.org/10.1088/0957-4484/27/36/364004>.
- Zheludkevich, M.L., Shchukin, D.G., Yasakau, K.A., Möhwald, H., Ferreira, M.G.S., 2007. Anticorrosion coatings with self-healing effect based on nanocontainers impregnated with corrosion inhibitor. *Chem. Mater.* 19 (3), 402–411. <https://doi.org/10.1021/cm062066k>.
- Zhu, A., Shi, P., Sun, S., Rui, M., 2019. Construction of rGO/Fe₃O₄/PANI nanocomposites and its corrosion resistance mechanism in waterborne acrylate-amino coating. *Prog. Org. Coat.* 133, 117–124. <https://doi.org/10.1016/j.porgcoat.2019.04.011>.